

Synthesis, Structure, and Photophysical Studies of Luminescent Two- and Three-Dimensional Gold–Thallium Supramolecular Arrays

Eduardo J. Fernández,[†] Peter G. Jones,[‡] Antonio Laguna,^{*§} José M. López-de-Luzuriaga,[†] Miguel Monge,[†] Javier Pérez,[†] and M. Elena Olmos[†]

Departamento de Química, Universidad de la Rioja, Grupo de Síntesis Química de La Rioja, UA-CSIC, Complejo Científico Tecnológico, 26006 Logroño, Spain, Institut für Anorganische und Analytische Chemie der Technischen Universität, Postfach 3329, D-38023 Braunschweig, Germany, and Departamento de Química Inorgánica, Instituto de Ciencia de Materiales de Aragón, Universidad de Zaragoza-CSIC, 50009 Zaragoza, Spain

Received September 10, 2001

The reactions of tetrahydrofuran solutions of $\text{NBu}_4[\text{AuR}_2]$ ($\text{R} = \text{C}_6\text{F}_5, \text{C}_6\text{Cl}_5$) with TIPF_6 and 4,4'-bipyridine lead to the synthesis of the luminescent materials $[\text{Ti}(\text{bipy})]_2[\text{Au}(\text{C}_6\text{F}_5)_2]_2$ **1** and $[\text{Ti}(\text{bipy})][\text{Ti}(\text{bipy})_{0.5}(\text{thf})][\text{Au}(\text{C}_6\text{Cl}_5)_2]_2$ **2** in high yield. The structures of these complexes, as analyzed by X-ray diffraction, consist of planar polymers formed by repetition of $\text{Ti}-\text{Au}-\text{Au}-\text{Ti}$ (**1**) or $\text{Ti}-\text{Au}-\text{Ti}'-\text{Au}$ (**2**) moieties linked through bidentate bridging bipy ligands. In complex **1** these layers are associated via $\text{Ti}\cdots\text{F}$ contacts between atoms of adjacent planes, whereas in complex **2** each two polymeric layers are linked through additional bridging bipy molecules. Both complexes are strongly luminescent at room temperature and at 77 K in the solid state, losing this characteristic in solution even at high concentrations. The luminescence is attributed to interactions between metal atoms which are strongly affected by their structural dispositions. DFT calculations are in accord with the observed experimental behavior, showing the nature of the orbitals involved in each transition. Detailed analyses reveal a substantial participation of the metals in the transition giving rise to the emission maxima, and also other more energetic bands in which the ligands are involved and which also give rise to these emissions. The obtained theoretical excitation spectra clearly match the experimental results.

Introduction

The term aurophilicity, coined to describe the strong closed-shell metal–metal interactions in gold(I) compounds,¹ has been extended in the past few years to wider concepts such as metallophilicity. In the case of gold, numerous examples of homoatomic associations and of those with other closed-shell metal ions have been reported, for example $\text{Cu}(\text{I})$,^{2a,3} $\text{Ag}(\text{I})$,^{3a} $\text{Tl}(\text{I})$,^{3b,4} $\text{Pb}(\text{II})$,^{4b} or $\text{Hg}(\text{II})$,⁵ giving rise to materials in which the metal–metal separations are shorter

than the sum of the van der Waals radii. The presence of these secondary interactions has allowed the synthesis of new species in which anomalous structural situations or the nonfulfillment of the Coulomb rule could be observed.⁶ The structures of such complexes involve a large variety of

* Author to whom correspondence should be addressed. E-mail: alaguna@posta.unizar.es.

[†] Universidad de la Rioja.

[‡] Institut für Anorganische und Analytische Chemie der Technischen Universität.

[§] Universidad de Zaragoza-CSIC.

- (1) Schmidbaur, H. *Gold Bull.* **1990**, 23, 11. Schmidbaur, H. *Chem. Soc. Rev.* **1995**, 24, 391. Scherbaum, F.; Grohmann, A.; Krüger, C.; Schmidbaur, H. *Angew. Chem., Int. Ed. Engl.* **1988**, 27, 1544. Schmidbaur, H. *Gold Bull.* **2000**, 33, 1.
- (2) Chan, C. K.; Guo, C. X.; Cheng, K. K.; Li, D.; Che, C. C. *J. Chem. Soc., Dalton Trans.* **1994**, 3677.

- (3) (a) See, for example: Fernández, E. J.; López-de-Luzuriaga, J. M.; Monge, M.; Rodríguez, M. A.; Crespo, O.; Gimeno, M. C.; Laguna, A.; Jones, P. G. *Chem. Eur. J.* **2000**, 6, 636 and references therein. (b) Burini, A.; Bravi, R.; Fackler, J. P., Jr.; Galassi, R.; Grant, T. A.; Omary, M. A.; Pietroni, B. R.; Staples, R. J. *Inorg. Chem.* **2000**, 39, 3158. (c) Fernández, E. J.; Gimeno, M. C.; Laguna, A.; López-de-Luzuriaga, J. M.; Monge, P.; Pyykkö, P.; Sundholm, D. *J. Am. Chem. Soc.* **2000**, 122, 7287.
- (4) (a) Wang, S.; Fackler, J. P., Jr.; King, C.; Wang, J. C. *J. Am. Chem. Soc.* **1988**, 110, 3308. (b) Wang, S.; Garzón, G.; King, C.; Wang, J. C.; Fackler, J. P., Jr. *Inorg. Chem.* **1989**, 28, 4623. (c) Crespo, O.; Fernández, E. J.; Jones, P. G.; Laguna, A.; López-de-Luzuriaga, J. M.; Mendía, A.; Monge, M.; Olmos, E. *Chem. Commun.* **1998**, 2233. (d) Catalano, V. J.; Bennett, B. L.; Kar, H. M. *J. Am. Chem. Soc.* **1999**, 121, 10235.
- (5) Burini, A.; Fackler, J. P., Jr.; Galasi, R.; Grant, T. A.; Omary, M. A.; Rawashdeh-Omary, M. A.; Pietroni, B. R.; Staples, R. J. *J. Am. Chem. Soc.* **2000**, 122, 11264.
- (6) Bauer, A.; Schmidbaur, H. *J. Am. Chem. Soc.* **1996**, 118, 5450.

inorganic assemblies based on metallophilicity, from discrete molecules to extended linear chains of mono-,^{4c} di-,^{4a,b} tri-,⁵ or tetranuclear units,^{3c} mediated by gold–gold or gold–heterometal interactions.

From a theoretical point of view these situations are controversial, since no attractions would be expected between closed-shell species and strong ionic bonds are expected when they carry opposite electric charges.⁷ In these cases, it seems plausible that the aggregation occurs by interaction of Lewis-acid complexes with Lewis-base complexes, thus displaying mainly dative bonds between two adjacent units. Associated with these comments, we recently reported the synthesis, structural characterization, and photophysical studies of extended linear chains formed in the reaction of the complex $[\text{Au}(\text{C}_6\text{F}_5)_2]^-$ with the Lewis acids AgClO_4 ^{3c} or TlNO_3 .^{4c} In both cases we observed interesting luminescence behavior based on the interactions between the various metal centers, verified through DFT calculations. Also, a mercury–gold complex recently reported by Fackler, Burini, and co-workers shows a luminescent monodimensional array of alternate trinuclear acid–base units.⁵

Mössbauer spectroscopic studies of related species indicate that the $[\text{Au}(\text{C}_6\text{F}_5)_2]^-$ groups do act as Lewis bases and the presence of perfluorophenyl groups seems to be the key factor for their donor properties.⁸ At this point, we wondered whether a change of the donor properties of the ligands attached to gold could effect a change in the assembly of the atoms, leading to different structures and photophysical properties, when the other conditions such as Lewis acids, ligands, and reaction pathways remain unchanged.

Here we report the synthesis, structural studies, and photophysical studies of the acid–base reaction between $[\text{NBu}_4][\text{AuR}_2]$ ($\text{R} = \text{C}_6\text{F}_5, \text{C}_6\text{Cl}_5$) complexes and thallium-(I) hexafluorophosphate in the presence of 4,4'-bipyridine, leading to novel 2- and 3-dimensional heterometallic gold–thallium arrays.

Experimental Section

Instrumentation. Infrared spectra were recorded in the 4000–200 cm^{-1} range on a Perkin-Elmer FT-IR spectrum 1000 spectrophotometer, using Nujol mulls between polyethylene sheets. C,H,N analyses were carried out with a C. E. Instrument EA-1110 CHNS-O microanalyzer. Mass spectra were recorded on a HP-5989B mass spectrometer API-electrospray with interface 59987A. ¹H, ¹⁹F NMR spectra were recorded on a Bruker ARX 300 in $(\text{CD}_3)_2\text{CO}$ solutions. Chemical shifts are quoted relative to SiMe_4 (¹H external) and CFCl_3 (¹⁹F external). UV–vis absorption spectra were obtained on a Shimadzu UV-2401 PC UV–visible recording spectrophotometer in acetone solutions ($\sim 4 \times 10^{-4}$ M). Excitation and emission spectra were recorded on a Perkin-Elmer LS-50B luminescence spectrometer. Acetone for photophysics was distilled over potassium permanganate and degassed before use. Emission lifetime measurements were performed with an Oriel 79110 N₂ laser system (pulse energy $500 \pm 20\%$ mJ, pulse output 337.5 nm, 5 ns). The emission signals were detected by a Hamamatsu R-1398 photomultiplier tube and recorded on a Tektronix model TDS-250

digital oscilloscope. Error limits are estimated: λ (± 0.1 nm); t ($\pm 7\%$).

Preparation of $[\text{Tl}(\text{bipy})_2][\text{Au}(\text{C}_6\text{F}_5)_2]_2$ (1**) and $[\text{Tl}(\text{bipy})][\text{Tl}(\text{bipy})_{0.5}(\text{thf})][\text{Au}(\text{C}_6\text{Cl}_5)_2]_2$ (**2**)** (**bipy** = 4,4'-Bipyridine; **thf** = Tetrahydrofuran). To a solution of TlPF_6 (0.09 g, 0.26 mmol) and $\text{NBu}_4[\text{Au}(\text{C}_6\text{F}_5)_2]_2$ (0.20 g, 0.26 mmol for **1**) or $\text{NBu}_4[\text{Au}(\text{C}_6\text{Cl}_5)_2]_2$ (0.243 g, 0.26 mmol for **2**) in THF (30 mL) was added 'bipy' (0.049 g, 0.32 mmol). The solution was stirred for 30 min, and the solvent was evaporated in vacuo. The resulting solids were washed with a portion of CH_2Cl_2 (20 mL) and filtered, yielding complexes **1** (73%) and **2** (88%) as pale-yellow and red solids, respectively. Both products are stable to air and show good solubilities in acetone and tetrahydrofuran.

Crystals suitable for X-ray diffraction studies were obtained by slow diffusion of hexane into a concentrated solution of the complex in acetone (**1**) or in tetrahydrofuran (**2**). For **1** the mass spectrum (ES[−]) shows $[\text{Au}(\text{C}_6\text{F}_5)_2]^-$ at $m/z = 531$ (100%) and (ES⁺) the Tl^+ ion at $m/z = 204$ (8%). For **2** the mass spectrum (ES[−]) shows $[\text{Au}(\text{C}_6\text{Cl}_5)_2]^-$ at $m/z = 695$ (100%). Elemental analysis (%) calcd for **1** ($\text{C}_{44}\text{H}_{16}\text{Au}_2\text{Tl}_2\text{F}_{20}\text{N}_4$): C, 29.63; H, 0.90; N, 3.14. Found: C, 30.23; H, 0.72; N, 3.06. Elemental analysis (%) calcd for **2** ($\text{C}_{43}\text{H}_{20}\text{Au}_2\text{Tl}_2\text{Cl}_{20}\text{N}_3\text{O}$): C, 24.52; H, 0.96; N, 1.99. Found: C, 24.57; H, 1.02; N, 2.35. ¹⁹F NMR (282 MHz, 298 K, $(\text{CD}_3)_2\text{CO}$): $\delta -114.8$ (m, *o*-F), $\delta -163.7$ (t, $J(\text{FF}) = 19.9$ Hz, *p*-F), $\delta -164.7$ (m, *m*-F). ¹H NMR for **1** (300 MHz, 298 K, $(\text{CD}_3)_2\text{CO}$): $\delta 8.7$ (d, $J(\text{HH}) = 6$ Hz, H-33' bipy), $\delta 7.7$ (d, $J(\text{HH}) = 6$ Hz, H-22' bipy). ¹H NMR for **2** (300 MHz, 298 K, $(\text{CD}_3)_2\text{CO}$): $\delta 8.7$ (d, $J(\text{HH}) = 6$ Hz, H-33' bipy), $\delta 7.7$ (d, $J(\text{HH}) = 6$ Hz, H-22' bipy), $\delta 3.42$ (m, H-2 thf) $\delta 1.85$ (m, H-3 thf).

Crystallography. The crystals were mounted in inert oil on glass fibers and transferred to the cold gas stream of a Bruker SMART 1000CCD (**1**) or a Nonius Kappa CCD (**2**) diffractometer equipped with an Oxford Instruments low-temperature attachment. Data were collected using monochromated Mo K α radiation ($\lambda = 0.71073$ Å). Scan type: ω and ϕ . Absorption corrections: numerical (based on indexed faces) for **1**, multiscan for **2**. The structures were solved by the Patterson method (**1**) or direct methods (**2**) and refined on F^2 using the program SHELXL-97.¹⁰ All non-hydrogen atoms were refined anisotropically. Hydrogen atoms were included using a riding model. Further details of the data collection and refinement are given in Table 1. Selected bond lengths and angles are collected in Tables 2 and 3.

Computational Methods. The molecular structures used in the theoretical studies of $[\text{Tl}(\text{py})_2][\text{Au}(\text{C}_6\text{H}_5)_2][\text{Au}(\text{C}_6\text{H}_5)_2][\text{Tl}(\text{py})_2]$ **1a** and $[\text{Tl}(\text{py})_2][\text{Au}(\text{C}_6\text{H}_5)_2][\text{Tl}(\text{py})(\text{H}_2\text{O})][\text{Au}(\text{C}_6\text{H}_5)_2]$ **2a** were taken from the X-ray diffraction results for $[\text{Tl}(\text{bipy})_2][\text{Au}(\text{C}_6\text{F}_5)_2]_2$ **1** and $[\text{Tl}_2(\text{bipy})_{1.5}(\text{thf})][\text{Au}(\text{C}_6\text{Cl}_5)_2]_2$ **2**, respectively. Keeping all distances, angles, and dihedral angles frozen, single-point DFT calculations were performed on the models. In both the single-point ground-state calculations and the subsequent calculations of the electronic excitation spectra, the default Beck–Perdew (B–P) functional^{11–13} as implemented in TURBOMOLE¹⁴ was used. The excitation energies were obtained at the density functional level using the time-dependent perturbation theory approach (TD-DFT),^{15–19} which is a density-functional-theory generalization of

(7) Pyykkö, P. *Chem. Rev.* **1997**, *97*, 597.

(8) Moss, K.; Parish, R. V.; Laguna, A.; Laguna, M.; Usón, R. *J. Chem. Soc., Dalton Trans.* **1983**, 2071.

(9) Usón, R.; Laguna, A. *Coord. Chem. Rev.* **1986**, *70*, 1.

(10) Sheldrick, G. M. *SHELXL-97, A program for crystal structure refinement*; University of Göttingen: Göttingen, Germany, 1997.

(11) Vosko, S. H.; Wilk, L.; Nusair, M. *Can. J. Phys.* **1980**, *58*, 1200.

(12) Perdew, J. P. *Phys. Rev. B* **1986**, *33*, 8822.

(13) Becke, A. D. *Phys. Rev. B* **1988**, *38*, 3098.

(14) Ahlrichs, R.; Bär, M.; Häser, M.; Horn, H.; Kölmel, C. *Chem. Phys. Lett.* **1989**, *162*, 165.

(15) Bauernschmitt, R.; Ahlrichs, R. *Chem. Phys. Lett.* **1996**, *256*, 454.

Table 1. Details of Data Collection and Structure Refinement for Complexes **1** and **2**

compound	1	2
formula	C ₂₂ H ₈ AuF ₁₀ N ₂ Tl	C ₄₃ H ₂₀ Au ₂ Cl ₂₀ N ₃ OTl ₂
fw	891.64	2106.29
cryst syst	triclinic	triclinic
space group	P1	P1
color	yellow	orange
a (Å)	7.6998(6)	11.1100(1)
b (Å)	11.5556(8)	14.595(2)
c (Å)	12.8272(8)	18.496(3)
α (deg)	105.102(3)	96.633(5)
β (deg)	105.477(3)	96.634(5)
γ (deg)	90.314(3)	109.742(3)
V (Å ³)	1058.48(13)	2765.96(6)
Z	2	2
T (K)	143(2)	173(2)
μ(Mo Kα) (mm ⁻¹)	14.627	12.011
reflins collected	21228	38269
R(int)	0.0449	0.08
unique reflins	6178	12955
GOF on F ²	1.025	1.114
Final R indices [I > 2σ(I)]: R1, wR2	0.0209, 0.0461	0.0467, 0.1123

Table 2. Selected Bond Lengths (Å) and Angles (deg) for Complex **1**

Au–C(21)	2.048(3)	Au–C(11)	2.049(3)
Au–Tl	3.0161(2)	Au–Au#1 ^a	3.4092(3)
Tl–N(31)	2.655(2)	Tl–N(41)	2.785(3)
Tl–F(2)#2	3.1704(18)	Tl–F(1)#2	3.1739(16)
C(21)–Au–C(11)	177.60(10)	C(21)–Au–Tl	85.72(7)
C(11)–Au–Tl	92.31(7)	C(21)–Au–Au#1	83.61(7)
C(21)–Au–Au#1	98.07(7)	Tl–Au–Au#1	164.925(6)
N(31)–Tl–N(41)	89.27(8)	N(31)–Tl–Au	96.27(8)
N(41)–Tl–Au	128.96(7)	N(41)–Tl–F(2)#2	140.78(6)
Au–Tl–F(2)#2	79.07(4)	N(31)–Tl–F(1)#2	79.61(6)
N(41)–Tl–F(1)#2	159.15(6)	Au–Tl–F(1)#2	74.42(3)
F(2)#2–Tl–F(1)#2	49.94(4)	C(12)–F(1)–Tl#2	127.56(15)
C(13)–F(2)–Tl#2	125.48(15)		

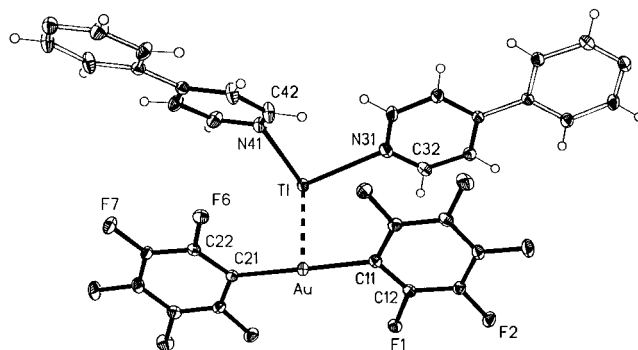
^a Symmetry transformations used to generate equivalent atoms: #1, $-x + 1, -y + 1, -z + 1$; #2, $-x + 2, -y + 1, -z + 1$.

the Hartree–Fock linear response (HF-LR) or random phase approximation (RPA) method.²⁰

In all calculations, the Karlsruhe split-valence quality basis sets²¹ augmented with polarization functions²² were used (SVP). The Stuttgart effective core potentials in TURBOMOLE were used for Au²³ and Tl.²⁴ Calculations were performed assuming *C_i* symmetry for **1** and *C₁* for **2**.

Results and Discussion

The heterometallic complexes [Au(C₆F₅)₂]₂[Tl(bipy)]₂ **1** and [Tl₂(bipy)_{1.5}(thf)][Au(C₆Cl₅)₂]₂ **2** (bipy = 4,4'-bipyridine; thf = tetrahydrofuran) were prepared by addition of TlPF₆ and 4,4'-bipyridine to a tetrahydrofuran solution of the

**Figure 1.** Asymmetric part of the polymeric structure of complex **1** with the labeling scheme of the atom positions.

gold(I) precursors [NBu₄][AuR₂] (R = C₆F₅ **1**; C₆Cl₅ **2**). The complexes were isolated as pale-yellow **1** and red **2** solids soluble in acetone and tetrahydrofuran and insoluble in diethyl ether and hexane. Solutions of both complexes are stable to air and moisture for days or weeks. Their elemental analyses and physical and spectroscopic properties are in accordance with the proposed stoichiometry. In particular, the conductivity measurements, and also the solution-state NMR spectroscopy, indicate a dissociative equilibrium between the positive and negative parts of each molecule, consistent with an ionic formulation as 1:1 electrolyte. Thus, the ¹⁹F NMR spectrum of **1** resembles that of the precursor complex [NBu₄][Au(C₆F₅)₂], while the ¹H NMR spectra in acetone solutions of **1** and **2** show the signals corresponding to the bipyridine ligands at 7.76 (AA' part) and 8.73 ppm (XX' part) (³J = 6.17 Hz). The latter are similar to those of the free ligand, which indicates that the dissociative equilibria in solution also involve the nitrogen-donor ligands. Also, in the case of complex **2**, two multiplets at 3.42 and 1.85 ppm can be assigned to the inequivalent protons of the thf molecule, whose integration is in agreement with the proposed stoichiometry. The IR spectra in Nujol mulls show, among others, absorptions arising from the C₆F₅²⁵ and C₆Cl₅²⁶ groups bonded to gold(I) at 1503, 957, and 783 cm⁻¹ for **1** and at 838 and 615 cm⁻¹ for **2**, respectively. Besides, in both derivatives, the Tl–N stretching mode appears at 371 **1** and 374 cm⁻¹ **2**, and in the case of **2**, a band of medium intensity is found at 350 cm⁻¹ and assigned to the ν(Tl–O) vibration.

The crystal structures of complexes **1** and **2** have been established by X-ray diffraction studies and show interesting structural differences. The asymmetric unit in **1** contains an [Au(C₆F₅)₂]⁻ unit (Au–C(11) = 2.049(3), Au–C(21) = 2.048(3) Å) and a thallium atom bonded to two bridging bipyridine ligands (Tl–N(31) = 2.655(2), Tl–N(41) = 2.785(3) Å) (Figure 1). These units are held together through a strong unsupported Au–Tl interaction of 3.0161(2) Å, shorter than the sum of thallium and gold metallic radii (3.034 Å) and also shorter than those found in [Tl(OPPh₃)₂][Au(C₆F₅)₂] (3.0358(8) and 3.0862(8) Å), the only example

- (16) Bauernschmitt, R.; Ahlrichs, R. *J. Chem. Phys.* **1996**, *104*, 9047.
 (17) Bauernschmitt, R.; Häser, M.; Treutler, O.; Ahlrichs, R. *Chem. Phys. Lett.* **1997**, *264*, 573 and references therein.
 (18) Gross, E. K. U.; Kohn, W. *Adv. Quantum Chem.* **1990**, *21*, 255.
 (19) Casida, M. E. In *Recent advances in density functional methods*; Chong, D. P., Ed.; World Scientific: Singapore, 1995; Vol. 1.
 (20) Olsen, J.; Jørgensen, P. In *Modern electronic structure theory*; Yarkony, D. R., Ed.; World Scientific: River Edge, NJ, 1995; Vol. 2.
 (21) Schäfer, A.; Horn, H.; Ahlrichs, R. *J. Chem. Phys.* **1992**, *97*, 2571.
 (22) Dunning, T. H., Jr. *J. Chem. Phys.* **1994**, *100*, 5829.
 (23) Andrae, D.; Haeussermann, U.; Dolg, M.; Stoll, H.; Preuss, H. *Theor. Chim. Acta* **1990**, *77*, 123.
 (24) Kuechle, W.; Dolg, M.; Stoll, H.; Preuss, H. *Mol. Phys.* **1991**, *74*, 1245.

- (25) Usón, R.; Laguna, A.; Laguna, M.; Manzano, B. R.; Jones, P. G.; Sheldrick, G. M. *J. Chem. Soc., Dalton Trans.* **1984**, 285.
 (26) Usón, R.; Laguna, A.; Laguna, M.; Manzano, B. R.; Tapia, A. *Inorg. Chim. Acta* **1985**, *101*, 151.

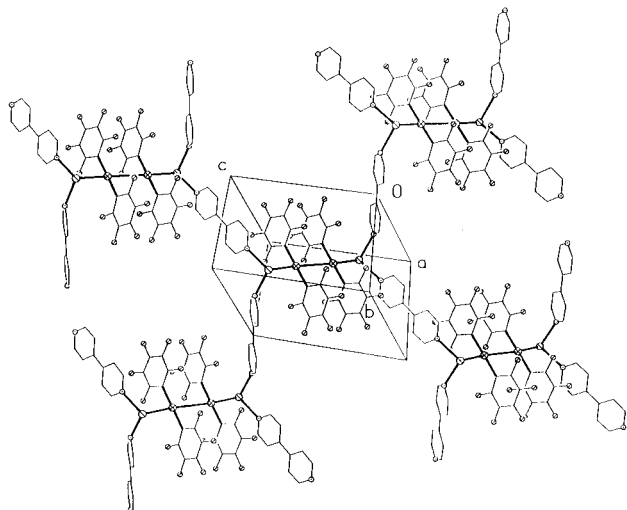


Figure 2. Polymeric layer structure of complex **1**. H atoms are omitted for clarity.

Table 3. Selected Bond Lengths (Å) and Angles (deg) for Complex **2**

Tl(1)–N(1)	2.680(7)	Tl(1)–N(2)	2.702(7)
Tl(1)–Au(1)	3.0323(4)	Tl(1)–Au(2)#1 ^a	3.0534(4)
Tl(2)–N(3)	2.724(7)	Tl(2)–O(1)	2.781(7)
Tl(2)–Au(2)	3.0485(4)	Tl(2)–Au(1)	3.0540(4)
Au(1)–C(7)	2.052(8)	Au(1)–C(1)	2.050(8)
Au(2)–C(13)	2.051(7)	Au(2)–C(19)	2.062(7)
Au(2)–Tl(1)#2	3.0534(4)	Tl(1)–Cl(6)	3.550(2)
Tl(1)–Cl(20)#2	3.556(2)	Tl(2)–Cl(5)	3.449(2)
Tl(2)–Cl(6)	3.755(2)	Tl(2)–Cl(11)	3.482(2)
Tl(2)–Cl(16)	3.769(2)		
N(1)–Tl(1)–N(2)	114.9(2)	N(1)–Tl(1)–Au(1)	91.74(16)
N(2)–Tl(1)–Au(1)	99.31(15)	N(1)–Tl(1)–Au(2)#1	85.57(17)
N(2)–Tl(1)–Au(2)#1	96.89(15)	Au(1)–Tl(1)–Au(2)#1	163.163(14)
N(3)–Tl(2)–O(1)	82.8(3)	N(3)–Tl(2)–Au(2)	112.54(15)
O(1)–Tl(2)–Au(2)	95.70(17)	N(3)–Tl(2)–Au(1)	101.01(15)
O(1)–Tl(2)–Au(1)	125.31(17)	Au(2)–Tl(2)–Au(1)	129.973(13)
C(7)–Au(1)–C(1)	173.9(3)	C(7)–Au(1)–Tl(1)	86.4(2)
C(1)–Au(1)–Tl(1)	91.2(2)	C(7)–Au(1)–Tl(2)	82.57(18)
C(1)–Au(1)–Tl(2)	103.2(2)	Tl(1)–Au(1)–Tl(2)	133.773(13)
C(13)–Au(2)–C(19)	176.1(3)	C(13)–Au(2)–Tl(2)	76.69(18)
C(19)–Au(2)–Tl(2)	106.7(2)	C(13)–Au(2)–Tl(1)#2	93.41(19)
C(19)–Au(2)–Tl(1)#2	83.81(19)	Tl(2)–Au(2)–Tl(1)#2	160.993(13)

^a Symmetry transformations used to generate equivalent atoms: #1, $x + 1, y, z$; #2, $x - 1, y, z$.

to date of unsupported gold–thallium linear chains.^{4c} Additional Au–Au contacts of 3.4092(3) Å form linear, tetranuclear moieties displaying an unusual Tl–Au–Au–Tl arrangement where repulsive instead of attractive forces could be expected. These tetranuclear units further connected to generate an infinite two-dimensional structure, via the bidentate bipy ligands that each bridge two thallium centers of different tetranuclear units (Figure 2). Finally, adjacent planes are connected by two additional Tl⋯F contacts of 3.1704(18) and 3.1739(16) Å, involving two fluorine atoms of the same C₆F₅ ring. Including these contacts, we may describe the structure of **1** as an infinite three-dimensional polymer.

In the case of complex **2** the asymmetric unit contains four metal centers (instead of two as observed in **1**) with a Tl–Au–Tl–Au arrangement, displaying short metal–metal interactions in the range 3.0323(4)–3.0540(4) Å: two gold(I) atoms of linear [Au(C₆Cl₅)₂][−] units with Au–C

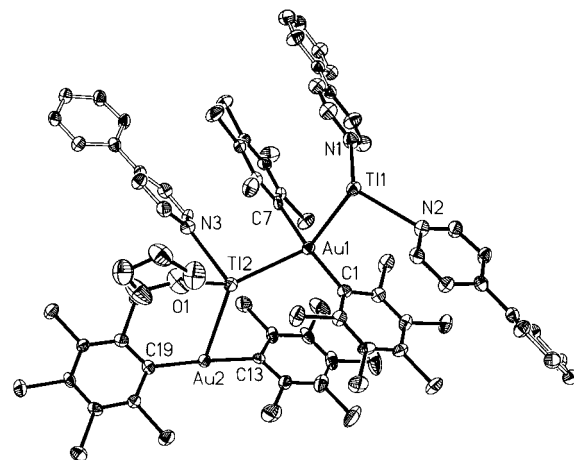


Figure 3. Asymmetric part of the polymeric structure of complex **2** with the labeling scheme of the atom positions.

distances in the range 2.050(8)–2.062(7) Å and two non-equivalent thallium centers (Figure 3). Whereas Tl(1) links two bipyridine ligands (Tl(1)–N(1) = 2.680(7) Å, Tl(1)–N(2) = 2.702(7) Å) and displays a trigonal bipyramidal geometry with a vacant equatorial coordination site, presumably associated with the stereochemically active lone pair, Tl(2) binds to a N atom of a bridging bipyridine (Tl(2)–N(3) = 2.724(7) Å) and to the oxygen center of a tetrahydrofuran molecule showing a Tl–O distance of 2.781(7) Å, similar to those observed in [(thf)₂Tl(μ-NC)Mn(CO)(dppm)₂][PF₆] (2.74(3) and 2.75(3) Å),²⁷ but appreciably longer than those in the related [Tl(OPPh₃)₂][Au(C₆F₅)₂] (2.483(3) and 2.550(4) Å)^{4c} with a strongly distorted tetrahedral geometry. The above-mentioned Au–Tl interactions infinitely extended, together with the presence of a bridging bipyridine ligand at each thallium, generate an infinite two-dimensional structure. Furthermore, the second bipyridine molecule bonded to Tl(1) connects each two planes as shown in Figure 4. Finally, while the thallium–halogen contacts between atoms of adjacent planes are not observed in this case, six Tl⋯Cl contacts (3.449(2)–3.769(2) Å) between atoms of the same linear chain may contribute to the stability of the system.

The electronic absorption spectra for both compounds shows similar features. Thus, in dilute acetone solutions ($\sim 5 \times 10^{-4}$ M) very low intensity absorptions at 387, 356, and 324 nm appear for **1** and at 385, 360, and 324 nm for **2**. It is likely that the band located at high energy arises from transitions localized in the π orbitals of the perhalophenyl groups, while in the low-energy region, the transitions probably involve orbitals of the gold centers. Similar behavior has been found by Lin and co-workers for aromatic phenyl groups²⁸ and by us in the tetranuclear complex [Au₂Ag₂(C₆F₅)₄(acetone)₂],^{3c} which shows a high-energy band at ~ 332 nm and low energy concentration dependent absorptions. Moreover, the electronic absorption spectra of the gold(I) precursor show bands at similar energies: at 383,

(27) Connelly, N. G.; Hicks, O. M.; Lewis, G. R.; Moreno, M. T.; Orpen, A. G. *J. Chem. Soc., Dalton Trans.* **1998**, 1913.

(28) Tang, S. S.; Chang, C. P.; Lin, I. J. B.; Liou, L. S.; Wang, J. C. *Inorg. Chem.* **1997**, *36*, 2294.

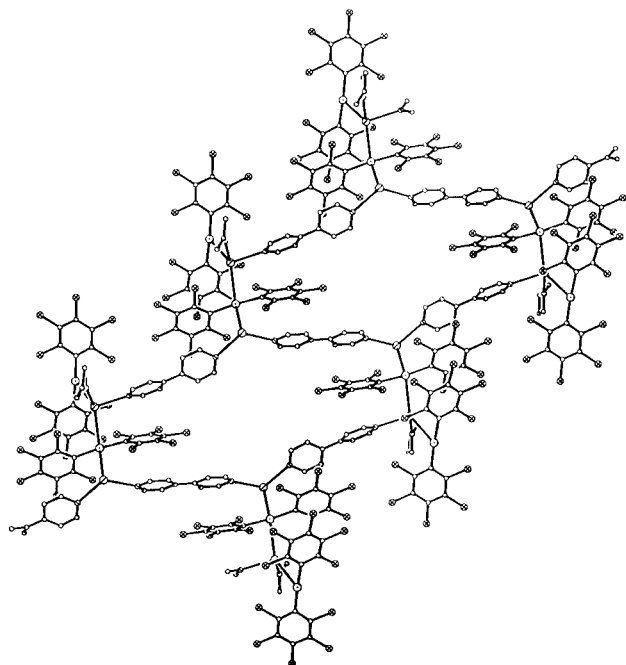


Figure 4. Side-on view of the double layer structure of complex **2**. H atoms are omitted for clarity.

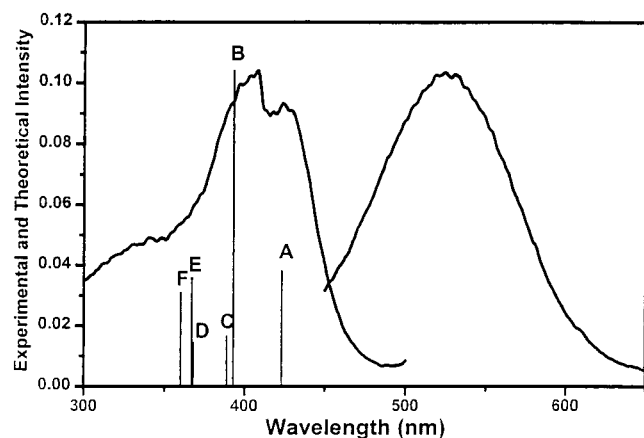


Figure 5. Excitation and emission spectra of compound **1** at room temperature in the solid state. Comparison between experimental excitation spectrum and theoretical oscillator strengths, f , from Table 6 for **1a** model.

353, and 324 nm for $\text{NBu}_4[\text{Au}(\text{C}_6\text{F}_5)_2]$ and at 384, 363, and 323 nm for $\text{NBu}_4[\text{Au}(\text{C}_6\text{Cl}_5)_2]$, data that are in accordance with the dissociation equilibrium of complexes **1** and **2** in acetone solutions that lead to free $[\text{AuR}_2]^-$ units.

The complexes show a very intense luminescence, both at room temperature (see Figures 5 and 6) and at 77 K in the solid state. Both compounds display a complicated excitation profile with maxima at 407 and 423 nm for **1** and at 394, 454, 464, and 534 nm for **2** that lead to a broad emission at 525 nm (half width (HW) = 3991 cm^{-1}) for **1** and 620 nm (HW = 2511 cm^{-1}) for **2** at room temperature, respectively. The luminescence in these complexes is temperature-dependent. In the case of the pentafluorophenyl derivative **1**, the emission is blue-shifted to 506.8 nm (HW = 3148 cm^{-1}) at 77 K, while in the pentachlorophenyl derivative **2**, the emission appears at lower energy (642.5 nm) with a half-width of 2140 cm^{-1} . The interesting blue

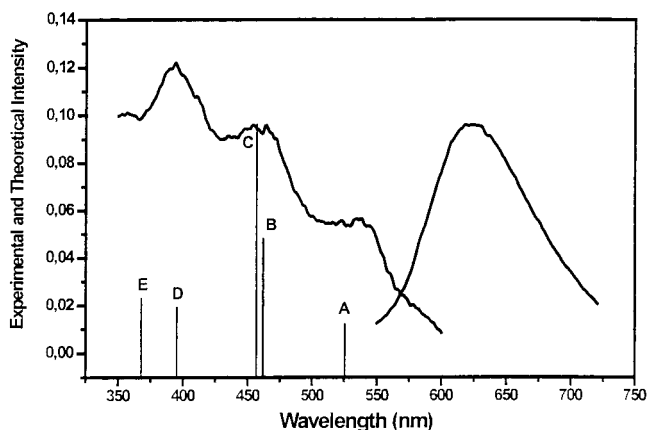


Figure 6. Excitation and emission spectra of compound **2** at room temperature in the solid state. Comparison between experimental excitation spectrum and theoretical oscillator strengths, f , from Table 7 for **2a** model.

shift of the emission band in **1** with decrease of temperature has been observed in some other luminescent complexes^{4b,29} and has been explained as a substantial dependence of the emission maxima on the environmental rigidity (*luminescence rigidochromism*). In contrast, the red shift observed for **2** with decrease of temperature has been found in other homo- and heteropolynuclear^{3b,c,30} complexes and related to a thermal contraction that leads to a reduction in the metal–metal distances along the chain, reducing the band gap energy. Thus, along with these comments, it seems clear that the different structures of both complexes have a significant influence on their luminescence properties and, taking into account that the precursor complexes and ligands are not luminescent under the same conditions, the metal–metal interactions seem to be responsible for the transitions that give rise to the light emissions. Moreover, when the products are dissolved in deoxygenated acetone or chloroform, the colors of the solids disappear and the resultant colorless solutions show only those assigned to the free bipyridine ligands (excitation = 209 nm; maximum emission = 341 nm) and bis(perhalophenyl)gold(I) units (C_6F_5 , excitation = 332, emission = 405 nm; C_6Cl_5 , excitation = 321, emission = 460 nm). Nevertheless, evaporation of the solvents regenerates the color of the complexes and their optical properties indicating, perhaps, that in both complexes the interactions responsible for the luminescence are lost in solution. Interestingly, an increase in the concentrations of both samples does not produce shifts in the excitation or emission bands. These results differ from those previously described by us in a recent paper,^{3c} in which the deviation from Lambert–Beer's law when the concentration increases was assigned to a molecular aggregation process in fluid solution of tetranuclear $[\text{Au}_2\text{Ag}_2(\text{C}_6\text{F}_5)_4(\text{OCMe}_2)_2]$ units through gold–gold interactions. It seems plausible that the tetranuclear units Tl–Au–Au–Tl in complex **1** and Au–Tl–Au–Tl in complex **2** are no longer present in solution even at higher concentrations.

(29) (a) Lees, A. *J. Chem. Rev.* **1987**, *87*, 711. (b) Ferrandi, G. J. *Elements of Inorganic Photochemistry*; John Wiley & Sons: New York, 1988.

(30) Van Zyl, W. E.; López-de-Luzuriaga, J. M.; Fackler, J. P., Jr. *J. Mol. Struct.* **2000**, *516*, 99.

Table 4. Population Analysis for the [Tl(Py)₂]⁺⋯[Au(C₆H₅)₂]⁻⋯[Au(C₆H₅)₂]⁻⋯[Tl(Py)₂] Model System. Contribution from Each Type of Atom to Occupied Orbitals

MO	% Au	% Tl	% N	% C	% H
HOMO (94a _g)	15.5	60.4	2.4	21.1	0.5
HOMO-1 (93a _g)	8.2	0.6	0.1	86.7	4.3
HOMO-2 (94a _u)	12.7	4.0	0.4	78.7	4.1
HOMO-3 (93a _u)	32.8	7.1		59.0	1.0
HOMO-4 (92a _u)	26.7	3.9	0.4	68.9	0.1
HOMO-5 (91a _u)	14.6	6.8	0.3	78.1	0.2
HOMO-6 (92a _g)	1.0	0.1		98.9	
HOMO-7 (90a _u)	8.1	5.5	0.7	85.6	
HOMO-10 (90a _g)	0.6	0.6		99.0	
HOMO-12 (88a _u)	87.7	7.4	3.0	1.8	

Table 5. Population Analysis for the [Tl(Py)₂]⁺⋯[Au(C₆H₅)₂]⁻⋯[Tl(Py)(H₂O)]⁺⋯[Au(C₆H₅)₂] Model System. Contribution from Each Type of Atom to Occupied Orbitals

MO	% Au	% Tl	% N	% C	% H
HOMO (172a)	1.5	4.9	0.1	93.3	0.1
HOMO-1 (171a)	13.7	1.5	0.2	83.0	1.6
HOMO-2 (170a)	51.21	14.2	2.2	30.9	1.2
HOMO-4 (168a)	6.1	0.2		93.3	0.4
HOMO-5 (167a)	16.3	0.7	0.05	82.5	0.4
HOMO-6 (166a)	7.9	0.7	0.3	87.0	3.9
HOMO-7 (165a)	13.7	0.3	0.5	85.4	
HOMO-9 (163a)	65.9	0.3		29.9	3.8
HOMO-10 (162a)	14.1	0.05	0.05	85.3	0.1

The presence of this interesting luminescent behavior for compounds **1** and **2** induced us to study in detail the transitions responsible for it. Thus, we performed single-point DFT calculations with two representative model systems of **1** and **2** such as [Tl(py)₂]⁺⋯[Au(C₆H₅)₂]⁻⋯[Au(C₆H₅)₂]⁻⋯[Tl(py)₂] (**1a**) and [Tl(py)₂]⁺⋯[Au(C₆H₅)₂]⁻⋯[Tl(py)(H₂O)]⁺⋯[Au(C₆H₅)₂] (**2a**), which were constructed from the X-ray diffraction results for complexes **1** and **2**, respectively, using phenyl rings instead of perhalophenyl ones in order to reduce the computational costs.

These calculations allowed us to carry out a study of the electronic structure of these compounds and a population analysis to check the contribution of each atom to each occupied orbital. The results are given in Tables 4 and 5, and the analysis of the highest occupied orbitals (94a_g, 93a_g, 94a_u, 93a_u, 92a_u, 91a_u, 92a_g, 90a_u, and 90a_g for model **1a**; 172a, 171a, 168a, 167a, 166a, 165a, and 162a for model **2a**) shows that they are mainly centered on carbon atoms; therefore, the highest occupied orbitals in both models are proposed to be located on phenyl and pyridine rings. Nevertheless, the 94a_g orbital is centered on thallium atoms (60%) and 88a_u is found on gold atoms (87.7%) for model **1a**, while 170a and 163a orbitals are mainly present on gold atoms (51.2% and 65.9%, respectively) for model **2a**. Besides, it can be emphasized that for 90a_u, 92a_u, and 93a_u orbitals from model **1a**, a growing 5d_{z²}σ* character in gold atoms appears when the energy of the orbitals increases (8.1%, 26.7%, and 32.8%, respectively); the same 5d_{z²}σ* character in gold atoms is observed for the 170a orbital (51.2%) in model **2a**.

As regards unoccupied orbitals, they cannot be analyzed by a population analysis, but we can check their shape. We can observe in both models two types of orbitals: ligand-centered orbitals (95a_g (LUMO) and 98a_u (LUMO+6) on model **1a** and 175a (LUMO+3) on model **2a**) and metal-

centered orbitals (99a_g (LUMO+8) on model **1a** and 178a (LUMO+6) on model **2a**). Thus, from single-point calculations it can be deduced that both the highest occupied orbitals and the lowest unoccupied ones enjoy a large contribution from the ligands and only in some of them are the contributions of the metals high. Therefore if, as is experimentally proposed, the luminescence of these complexes involves mainly orbitals of the metals, the calculations indicate that only a few of them are suitable for the transitions, and HOMO and LUMO are not included.

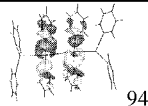
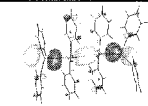
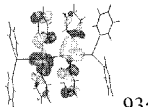
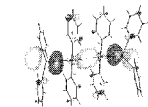
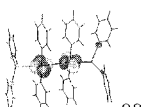


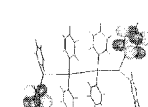
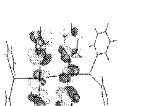
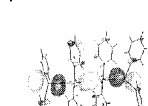
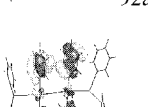
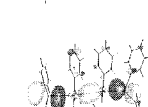
The theoretical confirmation of the participation in the photoluminescent properties of orbitals with high metallic character in complexes **1** and **2** comes from TD-DFT calculations, which allow us to predict theoretical excitations that can be compared in energy and intensity with the experimental ones, as well as the transitions between orbitals involved on each excitation. Thus, the first singlet excitation energies for the model systems **1a** and **2a** were calculated at the TD-DFT level (see Tables 6 and 7) as described in the computational methods section. In these, we cannot presently estimate the strength given by spin-orbit effects to the triplet excitations. Only singlet-singlet excitations were considered in these quasirelativistic calculations. No experimental singlet-triplet assignments were presented.

Taking into account their oscillator strengths (intensity) the most important theoretical excitations are B for model **1a** and C for model **2a**. Regarding model **1a**, excitation B gives a predicted excitation energy of 393.5 nm, comparable with the experimental excitation maximum at 407.7 nm. The most important contribution to excitation B is given by the transition between 93a_u (HOMO-3) and 99a_g (LUMO+8) orbitals. Concerning model **2a**, excitation C gives an excitation energy of 456.7 nm that clearly matches the experimental excitation maximum at 454.0 nm. Two contributions (170a → 178a and 167a → 175a) are mainly responsible for this excitation. As has been said before, orbitals 93a_u and 99a_g from model **1a** and 170a and 178a from model **2a** have a high metallic contribution, in accordance with the experimental assignment. In contrast, orbitals 167a and 175a are mostly ligand based.

Considering the shape of the orbitals in these transitions, orbitals 93a_u and 170a have a clear 5d_{z²}σ* character on gold atoms while 99a_g and 178a have a 6pσ* character and, therefore, the transitions between antibonding orbitals in both models would not produce a bond order enhancement among the metal centers and, thus, only a small structural distortion between ground and excited states is expected, in accordance with the fluorescence processes observed in the experimental spectra of **1** and **2** based on the small Stokes shift and in the lifetime measurements in the nanosecond time scale (τ₁ = 79 (2) ns, τ₂ = 256 (6) ns **1**; τ₁ = 80 (2) ns, τ₂ = 352 (7) ns **2**).

On the other hand, the rest of the theoretical excitations obtained are less intense for both models (30% or less for model **1a** and 50% or less for model **2a**) than the ones already described. Nevertheless, the excitation sets A-F (**1a**) and A-E (**2a**) give rise to theoretical excitation profiles that match the experimental ones.

Table 6. TD-DFT RPA Singlet-Excitation Calculations for [Ti(Py)₂]⁺⋯[Au(C₆H₅)₂]⁺⋯[Au(C₆H₅)₂]⁺⋯[Ti(Py)₂] (**1a**)

Excitation	$\lambda_{\text{calc.}}$ (nm) ^a	$\lambda_{\text{exp.}}$ (nm)	oscil. str. ^b (s)	CONTRIBUTIONS ^c	
A	423.8	423.5	0.380×10^{-1}		
	94 a _u → 99 a _g (87.2)				
	90 a _u → 97 a _g (5.8)				
B	393.5	407.7	0.104		
	93 a _u → 99 a _g (75.5)				
	88 a _u → 95 a _g (11.0)				
C	389.8	407.7	0.164×10^{-1}		
	88 a _u → 95 a _g (87.2)				
	93 a _u → 99 a _g (7.8)				
D	368.1		0.142×10^{-1}		
	90 a _g → 98 a _u (77.7)				
	92 a _u → 99 a _g (13.7)				
E	366.9		0.358×10^{-1}		
	92 a _u → 99 a _g (49.2)				
	91 a _u → 99 a _g (18.0)				
	88 a _u → 96 a _g (14.4)				
F	360.4		0.309×10^{-1}		
	90 a _u → 99 a _g (35.3)				
	91 a _u → 97 a _g (28.2)				
	94 a _u → 100 a _g (26.2)				

^a Value is $|\text{coeff}|^2 \times 100$. ^b Oscillator strength shows the mixed representation of both velocity and length representations. ^c Only the main contribution for each excitation is represented.

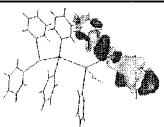

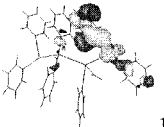
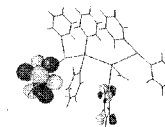
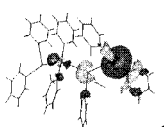
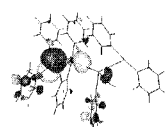
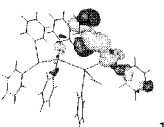
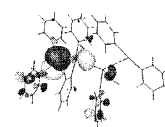
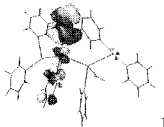
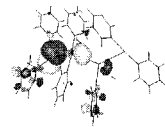
For compound **1**, the local maximum at 423.5 nm can be assigned to the theoretical excitation A (423.8 nm); the absolute maximum at 407.7 nm can be mainly assigned to the theoretical excitation B and to C, and the experimental shoulder from 300 to 360 nm can be assigned to excitations D, E, and F. As for the transitions that give rise to these secondary excitations, it is noteworthy that excitation A (94a_u → 99a_g) is similar to B because it comes from [Au(C₆H₅)₂]-based orbitals to metal-centered orbitals and, thus, can be viewed as L–MMCT (ligand–metal to metal charge transfer). Excitation C starts from orbital 88a_u, that is mainly localized on gold atoms (87%), and reaches a pyridine-based orbital 95a_g (MLCT) (metal to ligand charge transfer). Excitation D (90a_g → 98a_u) comes from C₆H₅ ligands to pyridine ligands (LLCT) (ligand to ligand charge transfer), and, finally, excitations E and F start from orbitals centered on the [Au(C₆H₅)₂] units and reach at the metal-based orbital 99a_g, similarly to the excitations A and B, although with a considerably reduced metal character in the starting orbitals.

Compound **2** has a more complicated excitation profile with four maxima located at 534.5, 464.0, 454.0, and 394.0 nm. For this pattern, the theoretical excitations can be divided into three groups: excitation A (525.5 nm) can be assigned to the local maximum at 534.5 nm; excitations B and C (461.8, 456.7 nm) correspond to the maxima at 464.0 and 454.0 nm, respectively; excitation D (395.2 nm) is assigned

to the local maximum that appears experimentally at 394.0 nm. Excitation A (171a → 178a) starts from the [Au(C₆H₅)₂] unit and goes to the metal-based orbital 178a (L–MMCT). Excitation B is the second most important transition, and it is similar in contributions to the most intense transition C; thus both excitations have the 170a → 178a transition from the 5d_{z²σ* gold-based orbital to the metal-based orbital 178a, that can be viewed as a M–MM–MCT (metal–metal to metal–metal charge transfer), and in addition the 167a → 175a transition, that starts from the [Au(C₆H₅)₂] unit and reaches the pyridine ligands (175a). Excitation D starts from the other [Au(C₆H₅)₂] unit and ends on an orbital in which the contribution of the metals is significant; finally, excitation E can be considered as a [Au(C₆H₅)₂] to the metals (178a) charge transfer.}

To conclude, from the TD-DFT calculations it can be claimed that the obtained theoretical excitations clearly match the experimental excitation spectra of compounds **1** and **2**. Besides, the excitation maxima (407.7 nm (theoretical 393.5 nm) **1** and 454.0 nm (theoretical 456.7 nm) **2**) are related to transitions in which the metal centers are involved and they are, presumably, responsible for the luminescent behavior. In spite of their different starting orbitals excitations E and F (**1a**) and D and E (**2a**) reach the same arrival orbitals (99a_g (**1a**) and 178a (**2a**), respectively) and can be viewed as metal+ligand to metal transitions. These provoke the same emission energy as in the low-energy excitations.

Table 7. TD-DFT RPA Singlet-Excitation Calculations for [Ti(Py)₂]⁺[Au(C₆H₅)₂]⁺[Au(Py)(H₂O)]⁺[Au(C₆H₅)₂] (2a)

Excitation	$\lambda_{\text{calc.}}$ (nm) ^b	$\lambda_{\text{exp.}}$ (nm)	oscil. str. ^c (s)	CONTRIBUTIONS ^d	
A	525.5	534.5	0.120×10^{-1}		
	171 a → 178 a (100)			171a	178a
B ^a	461.8	464.0	0.480×10^{-1}		
	167 a → 175 a (44.3)			167a	175
	170 a → 178 a (34.4)				
	163 a → 173 a (12.6)				
C ^a	456.7	454.0	0.960×10^{-1}		
	170 a → 178 a (43.8)			170a	178a
	167 a → 175 a (40.9)				
	170 a → 179 a (6.2)				
D	395.2	394.0	0.190×10^{-1}		
	167 a → 178 a (69.4)			167a	178a
	167 a → 179 a (13.5)				
E	367.9		0.230×10^{-1}		
	165 a → 178 a (44.7)			165a	178a
	162 a → 175 a (22.5)				
	165 a → 179 a (18.7)				

^a Note that for excitations B and C the same two transitions are important but in different order. ^b Value is $|\text{coeff}|^2 \times 100$. ^c Oscillator strength shows the mixed representation of both velocity and length representations. ^d Only the main contribution for each excitation is represented.

Even though perhalophenyl rings are substituted by phenyl ones, the good agreement between experimental and theoretical results is justified since the luminescence properties arise mainly from metal-based orbitals that are strongly dependent on the structural disposition. Nevertheless, the electronic properties of the halogens cannot be neglected, and they are currently under investigation.

Conclusions

(1) The use of different ligands at gold (C₆F₅ and C₆Cl₅) has a strong influence on the solid-state structure of compounds **1** and **2** when the other experimental conditions are unchanged.

(2) The photophysical behavior of compounds **1** and **2** is associated with the intermetallic interactions and the different structural arrangements.

(3) TD-DFT calculations clearly match the experimental excitation spectra of compounds **1** and **2**. They also imply that intermetallic interactions are mainly responsible for the transitions that give rise to luminescence although more energetic excitations in which the ligands are mostly involved also give rise to these emissions.

Acknowledgment. This work is dedicated to Professor P. Pyykkö on the occasion of his 60th birthday. We thank the Dirección General de Investigación Científica y Técnica (No. PB97-1010-C02-02) and the Fonds der Chemischen Industrie for financial support.

Supporting Information Available: X-ray crystallographic parameters in CIF format for compounds **1** and **2**. This material is available free of charge via the Internet at <http://pubs.acs.org>.

IC010961U